

Automated Classification of Brain MR Images using Extension with a Modified Relational Function

^{1,*}Chuin-Mu Wang and ²Shao-Wei Chu

Abstract

Image classification technique can process MRI multispectral information and help the doctors to accurately determine the lesion in the diagnosis. The Extension in the classification of brain MR images is improved in this study. First, we use the Target Generation Process based on Standard Deviation (TGPSD) to select the centers of the Extension interval in an unsupervised manner. Then we use the Particle Swarm Optimization (PSO) extension radius to find the best interval. And then, we use the best of the modified extension correlation function to classify the brain MR imaging. Next, gray matter, white matter and cerebral spinal fluid will be shown in each single image, respectively. Finally, the results are compared to *k*-means and FMRIB's automated segmentation tool; the superiority of modified Extension is evaluated and proved.

Keywords: MRI, Classification, Extension, Target Generation Process, Particle Swarm Optimization.

1. Introduction

The effective treatment is extremely important; furthermore, to adopt simple and accurate screening tools is also the key to early diagnosis of the presence of cancer because it can improve the self-examination in the medical. Magnetic resonance imaging technology, X-ray photography, fine needle aspiration cytology, digital X-ray photography, ultrasound, photography, computed tomography and immune contrast method are included in the current detection tools.

Magnetic resonance imaging technology becomes an indispensable medical clinical diagnosis and research work tool because it has its advantages of non-invasive and non-radiation damage; and with

the change in the imaging sequence it provides a wealth of information organization in recent years. Different parameters such as TR, TE, and PDI will produce images with different intensities in each brain tissue. The doctors can diagnose the myelination of the brain to determine congenital brain abnormalities, ischemic and hemorrhagic stroke, the elderly aging, brain tumors, brain trauma, central nervous system infections, brain white matter lesions, and the craniocervical junction lesions by multispectral images.

The charismatic of non-invasive and non-radiation damage with powerful imaging sequence variations provides rich tissue information. While the patient is arranged to process in MRI, which can produce a sequence of dimensional surfaces of the body image, we use the sequence of superimposed longitudinal section images to reconstruct the three-dimensional spatial structure of human organs. We capture a group of three to five images from the same slice of sequence which is a multispectral image.

Due to the development of computer technology, digital images process has a major breakthrough in software and hardware. Thus, the computer, digital image process technology is widely used in the diagnosis of various diseases, so there are a lot of people making a lot of help through the operation of the computer by the methods of [1-4], KFLM (Kalman Filter-based Linear Mixing) [5], OSP (Orthogonal Subspace Projection) [6-7], *k*-means, Fuzzy C-means [8-10], SVM (Support Vector Machine) [11], Neural Network [12-15], and Mean-Shift [16].

k-means clustering algorithm is the most representative. It is unsupervised from the sample, which is randomly selected as the initial cluster centers from sample data. Each datum will be calculated with the distance from the center in sequence, after that, the datum will be assigned to the nearest cluster after each iteration updates the cluster centers until converged. Aristidis Likas et al. [17] point out that *k*-means is easy to produce locally optimal solutions. The global *k*-means algorithm proposed uses the incremental way to find the desired *k* clusters in sequence to improve locally optimal solutions.

*Corresponding Author: Chuin-Mu Wang
(E-mail: cmwang@ncut.edu.tw)

¹Department of Computer Science and Information Engineering,
National Chin-Yi University of Technology, No.57, Sec. 2,
Zhongshan Rd., Taiping Dist., Taichung, Taiwan

²Department of Computer Science and Engineering, National Chung
Hsing University, No.250, Kuo Kuang Rd., South Dist., Taichung,
Taiwan

Extension theory [18-19] is based on its matter-element characteristics such as the target tissue intensity that calculates the range of interval used with sample points between the inner and the outer interval to reflect the most difference correlation functions. Thus, the effectiveness of the classification can be reached. The interval idea is more accurate than *k*-means because data points will be assigned to the nearest cluster center with the distance. However, the interval of extension can be applied to conclude the data points in the correct interval when each data point is nearest to border of interval in the extension concept. Therefore, it improves the effectiveness of classification.

Many creatures are gregarious species, so they rely on action groups to migrate and hunt; therefore, each individual that has played a significant role in the entire group was a highly efficient lifestyle. These common optimization algorithms based on Swarm-based are Ant Colony Optimization (ACO), Particle Swarm Optimization (PSO), and Artificial Bee Colony (ABC). PSO was proposed by Kennedy and Eberhart [20] in 1995. Many particles which present each potential solution search every possible solution in one optimization problem. Each particle will be memorized when it has searched. PSO is efficient in searching optimization because it also gets other particle searching experiments. The global optimal solution search swarm-based algorithm is the necessary key element which is the fitness assessment of the evolution of species. To evaluate fitness value, each particle will consider the best position of the single particle and the group of particles to find the better position; it will update its memory.

Detection Rate, False Alarm Rate and Correct Classification Rate are as a measure of the effectiveness of the standards and performance assessment basis to calculate classification results. This process that is the brain tissue of each division and a single tissue image are presented to show that the organization provides more rapid physicians with reference materials, more efficiently and accurately determining the lesion.

The definitions of Extension Theory are described in the Section 2. The method of this paper is proposed in the Section 3. The MR imaging classification experiment is to calculate classification rate and error rate in the Section 4. This paper is summarized in the Section 5.

2. Related Work

Extension [19, 21] is virtually a law or method that uses some formalized tools to resolve the discrepancy by way of qualitative and quantitative analysis. Matter-element theory and Extension set theory provide a basis for Extension classification of Extension Theory, of which Extension set is a

mathematical tool used to resolve the problems in Matter-elementary.

The matter - element is an abstract description of the interrelationship among objective matters covering the human beings, things and matters. Matters present various types of characteristics, each of which has a corresponding quantity value. Therefore, the name, characteristics and quantity value are described as three fundamental elements of matters. In defining Matter-element, a given name of the matter, is *N*; value of corresponding characteristics *C* is *V*. A Matter-element is defined below:

$$R = (N, C, V(N)) \tag{1}$$

Generally, a Matter-element has neither a characteristics *C*, nor a single quantity value *V*, so multi-dimensional matter-elements are most frequently used in Extension applications:

$$R = (N, C, V) = \begin{matrix} R_1 \\ R_2 \\ \vdots \\ R_n \end{matrix} = \begin{matrix} N, C_1, V_1 \\ , C_2, V_2 \\ , \vdots, \vdots \\ , C_n, V_n \end{matrix} \tag{2}$$

Let *U* as a universe, if $u \in U$ has a real number $K(u) \in (-\infty, +\infty)$ corresponding to any element *u* within *U*; then an Extension set *A* is defined as follows:

$$A\{(u, y) | u \in U, y = K(u) \in (-\infty, +\infty)\} \tag{3}$$

Where an Extension is set on *U*, $y=K(u)$ is relational function of *A*, and $K(u)$ is relational degree of *u* in connection with *A*.

Relational function is a major part of Extension in the applications, wherein the relational function is used to calculate the degree of similarity among matter-elements.

In a grayscale (single channel) image *G*, every pixel is defined as $G(x, y)$ that is a single value between 0 and 255 at location (x, y) in image *G*. A four classes ($C = 4$) case for classification, the Extension method needs *C* interval targets that are defined as $X_k = \langle a_k, b_k \rangle$ for $k = 1, 2, \dots, C$ where the a_k and b_k are minimal and maximal of *k*-th target, respectively. A $\bar{X}_k = \langle c_k, d_k \rangle$ is extensive interval of the *k*-th target X_k . The X_k and \bar{X}_k without public terminal, let

$$\alpha(G(x, y)) = \left| G(x, y) - \frac{a_k + b_k}{2} \right| - \frac{|b_k - a_k|}{2} \tag{4}$$

$$\beta(G(x, y)) = \left| G(x, y) - \frac{c_k + d_k}{2} \right| - \frac{|d_k - c_k|}{2} \tag{5}$$

$$K_k(G(x, y)) = \begin{cases} \frac{-\alpha(G(x, y))}{|a-b|} & \alpha < 0 \\ \frac{\alpha(G(x, y))}{\beta(G(x, y)) - \alpha(G(x, y))} & \alpha \geq 0 \end{cases} \quad (6)$$

Where $\alpha(G(x, y))$ and $\beta(G(x, y))$ are the Extension distance between $G(x, y)$ and X_k or \bar{X}_k , respectively.

If $K_k(G(x, y)) > 0$, $G(x, y)$ is assigned to X_k . If $K_k(G(x, y)) < -1$, $G(x, y)$ doesn't belong to X_k . If $-1 \leq K_k(G(x, y)) \leq 0$, the judgment of $G(x, y)$ within Extension interval must depend upon the other intervals of targets.

3. Extension with Modified Relational Function

A multispectral image I with size $L \times W$ has B bands, a pixel at location (x, y) ; an image I is represented as $I(x, y) = (b_1^{x,y}, b_2^{x,y}, \dots, b_B^{x,y})^T$, $x=1, 2, \dots, L, y=1, 2, \dots, W$.

The proposed method has three main parts: First, the standard deviation generating process is used to pick the right target pixel vectors as the cluster centers. Then the Extension correlation function of each tissue is defined by the cluster center. Next, the optimal solution of this function is calculated through the approximate particle swarm optimization algorithm. Finally, the best simple correlation function classification is used to classify. The targets are GM, WM and CSF categories. The number of classes C is 3.

3.1 Target Generation Process based on Standard Deviation (TGPSD)

Real data are normally distributed, and the information of stability universe should correctly belong to the class so that we select the characteristics of low similarity that complies to low standard deviation with the neighboring data to achieve the unsupervised. In this paper, we use TGPSD to define stability universes $X_k = \langle a_k, b_k \rangle$ that add the standard deviation to improve Target Generation Process [22]. The TGPSD is described as follows:

- 1). Let $t = 0$. For generation C targets, arbitrarily select a pixel (x, y) from the multispectral image I and consider the region $\Omega(x, y)$ of the point (x, y) as follows:

$$\Omega(x, y) = \{p(q, x) \mid p \leq x + y - 1 \leq q \leq y + 1\} \quad (7)$$

- 2.) Compute the mean μ_t and standard deviation σ_t of the $\Omega(x, y)$, as follows:

$$\mu_t = \frac{1}{|\Omega|} \sum_{b \in \Omega(x, y)} b \quad (8)$$

$$\sigma_t(x, y) = \frac{\sqrt{\frac{1}{|\Omega|} \sum_{b \in \Omega(x, y)} (b - \mu_t)^2}}{m \times \sigma_t} \quad (9)$$

- 3). Set $t = t + 1$. The membership function S_t is defined as Eq. (4). Calculate the membership $S_t(r, s)$ of all pixels $I(r, s)$ ($r = 1, 2, \dots, L; s = 1, 2, \dots, W$) in the whole image, as follows:

$$S_t(r, s) = 1 - \frac{1}{\sigma_{t-1} \sqrt{2\pi}} e^{-\frac{(I(r, s) - \mu_{t-1})^2}{2\sigma_{t-1}^2}} \quad (10)$$

- 4). Compute $F_t(r, s)$ as follows:

$$F_t(r, s) = \prod_{k=1}^t S_k(r, s) \quad (11)$$

- 5). Find the $I(r, s)$ that correspond to the maximum $F_t(r, s)$ as target $T_t = I(r, s)$, and update $\Omega(x, y) = \Omega(r, s)$. If $t = C$, let $E = \{T_1, T_2, \dots, T_t\}$ and terminate this method, otherwise go to step (2).

The membership S_t is shown in Fig. 1. The TGPSD can obtain the C targets that are more difference from an image I . Fig. 2 shows the four targets that are marked by a red circle.

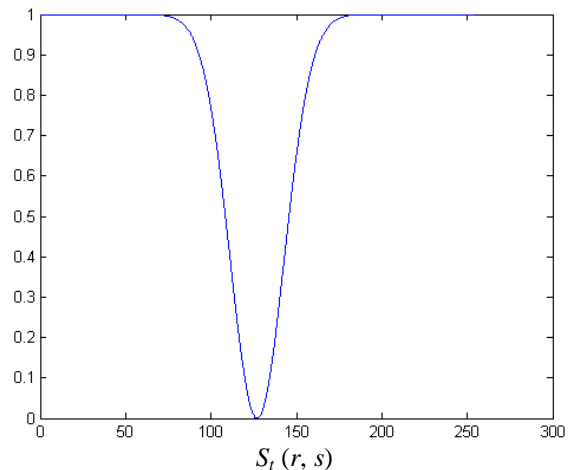


Figure 1: The membership function S_t .

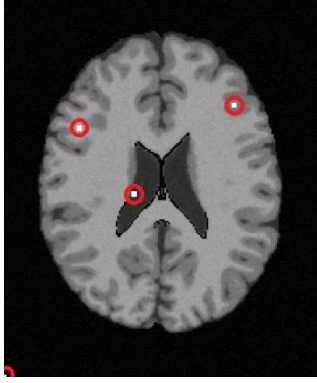


Figure 2: The four targets are generated by TGPSD.

3.2 The Modified Relational Function

Extension methods have been used in the classification of the MRI images, such as [19]. However, it will be calculated separately for each dimension in the original extension method, and then takes the maximum sum. The definition of Extension correlation function is assumed that each dimension feature is not related to each other.

In MRI images, the different spectral parameters are used to scan the brain in the same sliced position to obtain a sequence of images which are multispectral images. Its approach is different from the general image, which not only process information in a single image, but also deal with between the spectrum of the other images and information. Thus, in multispectral images, each pixel is composed by a vector, and every element represents different spectral characteristics in the vector.

Extension correlation function is calculated from the Euclidean distance in this study and used by the simple correlation function. The function is defined as follows:

$$K'_k(I(x, y), M_k, r_k) = \|I(x, y) - M_k\| \cdot r_k \quad (12)$$

Where M_k is the center of k -th target, and r_k is the radius. The M_k and r_k are optimized by the PSO in the next subsection. The relationship of the function K'_k is to illustrate in Fig. 3. The every pixel of image I is assigned to the one of the C classes by the modified relational function of Extension. A pixel $I(x, y)$ is assigned to q -th class by the following equation:

$$q_{(x,y)} = \arg \min_{k=1,2,\dots,C} K'_k(I(x, y), M_k, r_k) \quad (13)$$

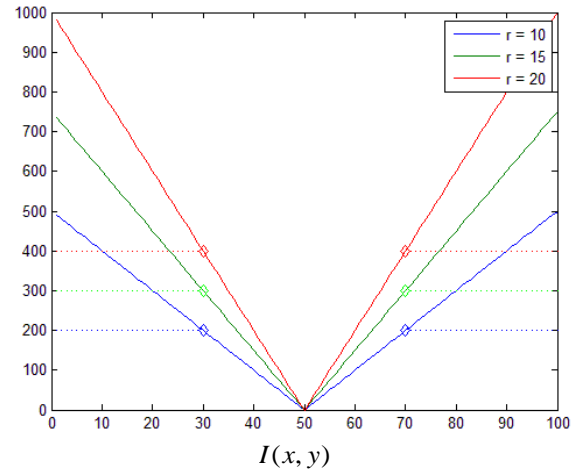


Figure 3: The relationship of the relational function K'_k .

3.3 Particle Swarm Optimization (PSO)

Particle Swarm Optimization is a kind of global swarm-based optimal solution search algorithms. Many particles which present each potential solution search every possible solution in one optimization problem. An individual particle is computed by fitness to get solved. Each particle memorizes the best solution as it is searching and if also can get the best solution in a group when other particles are searching. The group of particle is searching possible solutions by iterative and keeping memorizing in the iterative. This makes the particle moving in the search space, and also considers the position of the particle to be the best experience.

Let the set of particles is $R^i = \{r_1^i, r_2^i, \dots, r_N^i\}$, where the N is the number of the particles, and the i is i -th iteration. The r_j^i is the j -th particle in the i -th iteration. The set of speeds corresponding to R^i is $V^i = \{v_1^i, v_2^i, \dots, v_N^i\}$. The v_j^i is the speed of the j -th particle in the i -th iteration. The iteration times $ITER$ is set 20 and $N=10$. The f_j^i presents the fitness of j -th particle in the i -th iteration. The f_j^{best} is the best fitness of j -th particle until current iteration. The r_j^{best} is the best solution of j -th particle corresponding to f_j^{best} .

The f^{best} is the best fitness of all particle until current iteration. The r^{best} is the best solution corresponding to f^{best} . The PSO algorithm is described as follows:

- 1). Randomly initial the particle r_j^i and speed v_j^i for $j=1, 2, \dots, N$. and $i=1$.
- 2). Estimate the fitness f_j^i of each particle r_j^i in the following:

$$f_j^i = \sum_{k=1}^C K_k' (I(x,y) M_k r_p^i) \quad (14)$$

- 3). If the fitness $f_j^i < f_j^{best}$, then update the $f_j^{best} = f_j^i$ and $r_j^{best} = r_j^i$ for $\forall j = 1, 2, \dots, N$.
- 4). Find the best fitness $f^{best} = \min(f_j^{best})$, $\forall j = 1, 2, \dots, N$ and $r^{best} = r_z^{best}$, where $z = \arg \min_{j=1,2,\dots,N} (f_j^{best})$.
- 5). If $i < ITER$, calculate the equation 15 and 16. Then set $i=i+1$ and go to step 2. If $i = ITER$, then terminate.

$$v_j^{i+1} = v_j^i + c_1 \times \text{rand}(0,1) \times (\eta_j^{best} - r_j^i) + c_2 \times \text{rand}(0,1) \times (r_j^{best} - r_j^i) \quad (15)$$

$$r_j^{i+1} = r_j^i + v_j^{i+1} \quad (16)$$

The new v_j^{i+1} consist of current v_j^i , individual particle and social particle. The c_1 and c_2 are acceleration constants which set 0.5, and the $\text{rand}(0, 1)$ is a random function between 0 and 1.

4. Experimental Results

To evaluate the performance of the proposed method, a publicly simulated database of multi-spectral images is used for the first experiment in Section 4.1. The ground truth and simulated images are downloaded from the website (<http://brainweb.bic.mni.mcgill.ca/brainweb>) of the BrainWeb. In quantitative analysis, we used the receiver operating characteristic (ROC) to calculate the detection rate and false rate in Section 4.2. The final experiment is to test the proposed method on a real brain MR images in Section 4.3.

4.1 BrainWeb: Simulated Brain Database

BrainWeb simulated image shown in Fig. 4 is downloaded from the simulated brain database (<http://brainweb.bic.mni.mcgill.ca/brainweb>). It has been widely used in MRI classification research in the decade. There are a spectrum of simulated PD, T1 and T2, and the image size is 181×217 . The experiment will be based on the ground truth provided by BrainWeb in Fig. 5. It retains three major brain tissues, gray matter (GM), white matter (WM) and cerebral spinal fluid (CSF). The intensities are listed in Table 1 for the simulated images in Fig. 4.

In order to test the robustness of the proposed method, we mix the Rician Noise into the simulated images with 20dB, 15dB, 10dB and 5dB in Figs. 6, 7, 8, and 9, respectively. The classified results between 20dB and 5dB images by the proposed method are shown in Figs. 10, 11, 12 and 13, respectively.

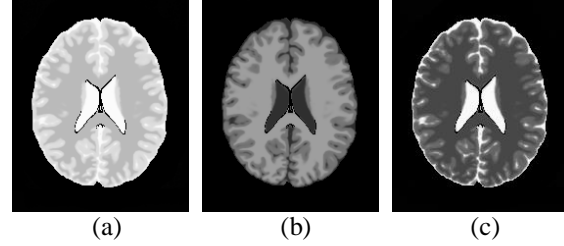


Figure 4: Three bands of simulated brain images from BrainWeb: (a)PD; (b)T1; (c)T2.

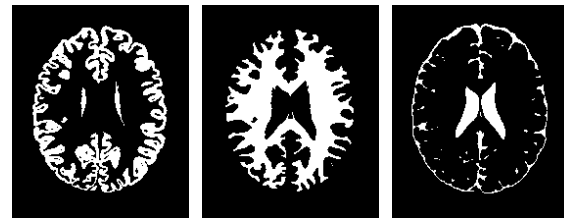


Figure 5: The ground truth of the simulated brain images.

Table 1: The gray level of the three main tissues from simulated brain images.

| Band # | GM | WM | CSF |
|--------|-----|-----|-----|
| PD | 218 | 184 | 248 |
| T1 | 111 | 150 | 45 |
| T2 | 101 | 71 | 248 |

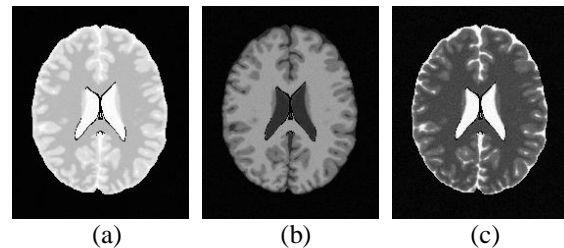


Figure 6: BrainWeb image for added noise with SNR=20db. (a)PD (b)T1 (c)T2.

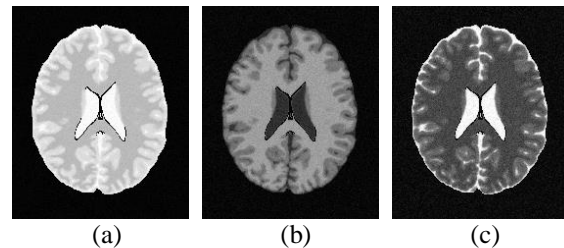


Figure 7: BrainWeb image for added noise with SNR=15db. (a)PD (b)T1 (c)T2.

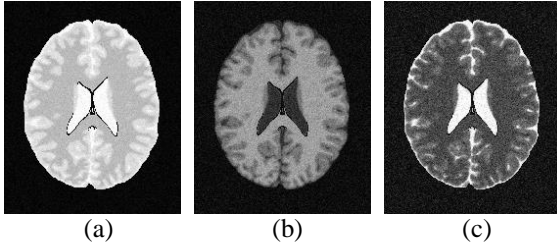


Figure 8: BrainWeb image for added noise with SNR=10db. (a)PD (b)T1 (c)T2.

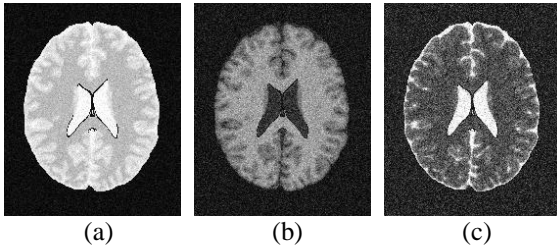


Figure 9: BrainWeb image for added noise with SNR=5db. (a)PD (b)T1 (c)T2.

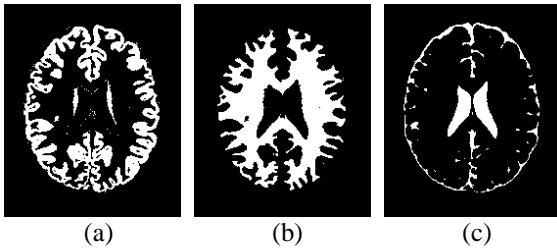


Figure 10: Classified results by proposed method for added 20db noise phantom images. (a)GM. (b)WM. (c)CSF.

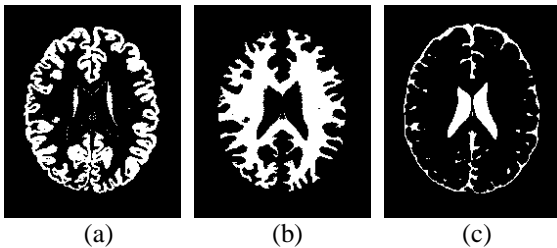


Figure 11: Classified results by proposed method for added 15db noise phantom images. (a)GM. (b)WM. (c)CSF.

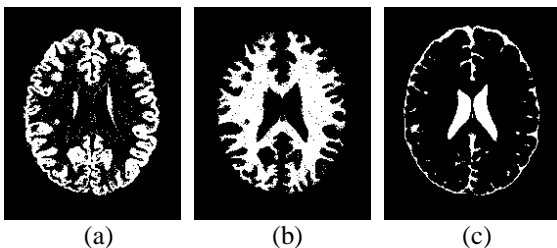


Figure 12: Classified results by proposed method for added 10db noise phantom images. (a)GM. (b)WM. (c)CSF.

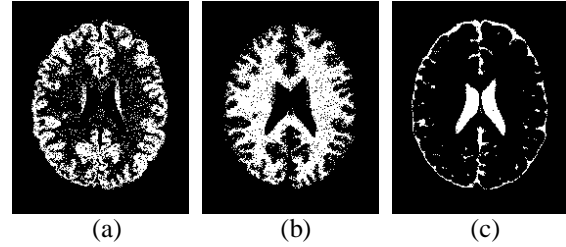


Figure 13: Classified results by proposed method for added 5db noise phantom images. (a)GM. (b)WM. (c)CSF.

4.2 Receiver Operating Characteristic (ROC)

Receiver Operating Characteristic [23] analysis, which is still one of a credible assessment methodology, has been used to evaluate the performance of classification and identification. The proposed method, *k*-means, and FAST (FMRIB's Automated Segmentation Tool) are evaluated by the detection rate and false rate of ROC in this experiment.

FAST (FMRIB's Automated Segmentation Tool) is established by the University of Oxford, Department of Clinical Neurology of Functional Magnetic Resonance Imaging Brain center, which specializes in brain MRI image, and combines Hidden Markov Random Field (HMRF) and Expectation Maximization (EM) algorithm into FAST automatic segmentation tool.

As the criteria for evaluation, detection rate $R_D(d_i)$ and false rate $R_F(d_i)$ are the most important in ROC. Each tissue classification result are all binary images, so it is easy to distinguish the classification of various organizations, which contain the detection rate and false rate point. Although these results can be determined by the naked eye, they will be a statistic with detection rate and false rate through the ROC. The experiment results will be further discussed, and the next ROC will be introduced gradually.

When evaluated for classification, ground truth usually has a standard result in the simulated image. Classification results are analyzed by the ground truth to get the results of pixel classification. Eq. (17) can calculate the detection rate of various tissues $R_D(d_i)$, and Eq. (18) can calculated the false rate of various tissues $R_F(d_i)$. All kinds of tissues can be shown in the $R_D(d_i)$ and $R_F(d_i)$.

$$R_D(d_i) = \frac{N_D(d_i)}{N(d_i)} \quad (17)$$

$$R_F(d_i) = \frac{N_F(d_i)}{N - N(d_i)} \quad (18)$$

$R_D(d_i)$ is the detection rate of tissue d_i . $R_F(d_i)$ is the false rate, $d=\{d_1, d_2, \dots, d_i\}$ ($i = 1, 2, \dots, C$), and $C=3$. The d_i is i -th tissue. N is the total number of pixels in the ground truth. $N_D(d_i)$ is the number of correct pixels for classification. $N_F(d_i)$ is the number of incorrect pixels for classification. $N(d_i)$ is the number of pixels with tissue d_i in ground truth.

The mean detection rate R_D and mean false rate R_F are defined as follows:

$$R_D = \sum_{i=1}^k R_D(d_i) p(d_i) \quad (19)$$

$$R_F = \sum_{i=1}^k R_F(d_i) p(d_i) \quad (20)$$

$$p(d_i) = \frac{N_D(d_i)}{N(d_i)} \quad (21)$$

The four multi-spectral images (between Figs. 6 and 9) are classified by using the proposed method for 100 execution times. The best, average, and worst of detection and false rate are listed in Tables 2 and 3, respectively. In Table 2, the proposed method obtains a higher detection rate between 20dB and 5dB. In Table 3, the false rates of average situation are less than 0.15.

The proposed method is compared to the k -means and FAST. In Table 4, the detection rates of the proposed method are more accurate than k -means and FAST between 20dB and 5dB.

Table 2: The detection rate of classification results by proposed method for 100 execution times.

| | 20dB | 15dB | 10dB | 5dB |
|---------|--------|--------|--------|--------|
| Average | 0.9684 | 0.9567 | 0.9370 | 0.8341 |
| Best | 0.9795 | 0.9723 | 0.9480 | 0.8671 |
| Worst | 0.9320 | 0.8919 | 0.8844 | 0.7128 |

Table 3: The false rate of classification results by proposed method for 100 execution times.

| | 20dB | 15dB | 10dB | 5dB |
|---------|--------|--------|--------|--------|
| Average | 0.0171 | 0.024 | 0.0445 | 0.101 |
| Best | 0.0106 | 0.0148 | 0.0332 | 0.0894 |
| Worst | 0.0364 | 0.0579 | 0.0645 | 0.1553 |

Table 4: The mean detection rate R_D of classification results by proposed method, k -means and FAST.

| | 20dB | 15dB | 10dB | 5dB |
|------------|--------|--------|--------|--------|
| Proposed | 0.9795 | 0.9723 | 0.9480 | 0.8671 |
| k -means | 0.9742 | 0.9662 | 0.9445 | 0.8531 |
| FAST | 0.8910 | 0.9459 | 0.6437 | 0.6365 |

4.3 The real brain MR images

Magnetic Resonance Imaging (MRI) images are taken from the department of radiology in Taichung Veterans General Hospital, and the machine is Signa 1.5-T SYS#GEMSO. Multi-spectral images are for brain magnetic resonance imaging, and the top of the image is the front proportion of the human body. The position of the image to the left and right way is opposite to the actual position of the human body. The magnetic field strength is 1.5-Tesla, and the size of each image is 256×256 pixels.

The real MR images were used for performance evaluation. They were acquired from ten patients with normal physiology. One example is shown in Figs. 14(a)-(e) with the same parameter values. Band 1 is the PD-weighted spectral image acquired by the pulse sequence $TR/TE = 2500ms/25ms$. Bands 2, 3 and 4 are T2-weighted spectral images acquired by the pulse sequences $TR/TE = 2500ms/50ms$, $TR/TE = 2500ms/75ms$ and $TR/TE = 2500ms/100ms$, respectively. Band 5 is the T1-weighted spectral image acquired by the pulse sequence $TR/TE = 500ms/11.9ms$. The tissues surrounding the brain, such as bone, fat and skin, are semi-automatically extracted using interactive thresholding and masking. The slice thickness of all the MR images is 6mm, and axial section was taken from GE MR 1.5T Scanner.

Gray matter, white matter and cerebral spinal fluid are the three major targets in the brain. These three tissue classifications of the proposed method, k -means, and FAST, are shown in the Figs. 15 to 17. Comparison of Figs. 15(c) and Fig. 17(c) shows that the classification of the proposed method performs significantly better than FAST in CSF. The k -means classification results in Fig. 16 is to take the best results because the k -means uses random initial cluster centers. Thus, the classification results are not stable.

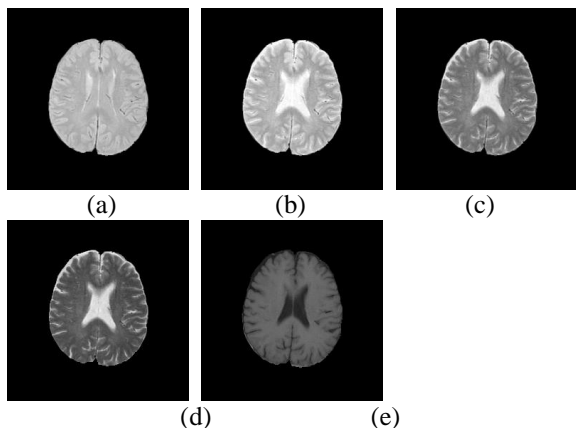


Figure 14: Five bands of real multi-spectral brain images:
 (a)Band 1: TR/TE=2500ms/25ms
 (b)Band 2: TR/TE=2500ms/50ms
 (c)Band 3: TR/TE=2500ms/75ms
 (d)Band 4: TR/TE=2500ms/100ms
 (e)Band 5: TR/TE=500ms/11.9ms.

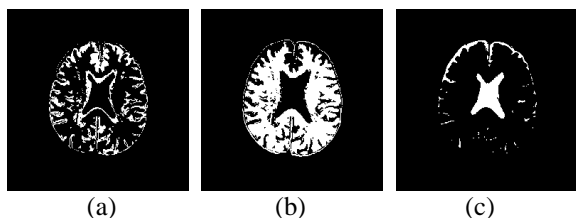


Figure 15: Classified results by proposed method for the image in Fig. 14. (a)GM. (b)WM. (c)CSF.

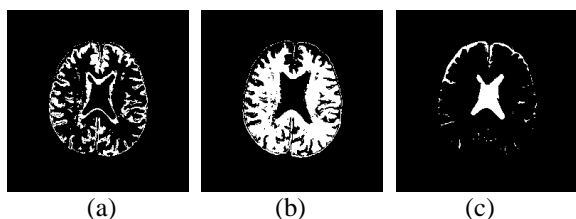


Figure 16: Classified results by *k*-means for the image in Fig. 14. (a)GM. (b)WM. (c)CSF.

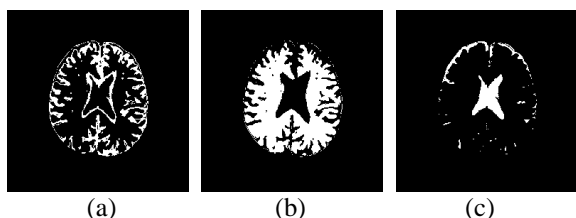


Figure 17: Classified results by FAST for the image in Fig. 14. (a)GM. (b)WM. (c)CSF.

5. Conclusions

This paper presented the Modified Relational Function of Extension for multi-spectral MR image classification. The proposed method consists of three processes, the Target Generation Process (TGP), Modified Relational Function and Particle Swarm Optimization. The set of potential targets is obtained by TGP from multi-spectral images. These targets are then classified by the Extension using modified relational functions. And the radiuses of the Extension intervals are optimized by PSO. The performance of the proposed method, *k*-means and FAST were measured experimentally using two sets of images. One is simulated brain images from BrainWeb. The other is real brain MR images. Experimental results show that the proposed method has more effective classification for multi-spectral MR image than *k*-means and FAST.

References

- [1]. B. Johnston, M. S. Atkins, B. Mackiewich, and M. Anderson, "Segmentation of Multiple Sclerosis Lesions in Intensity Corrected Multispectral MRI," IEEE Transactions on Medical Imaging, vol. 15, no. 2, pp. 154-169, April 1996.
- [2]. M. Stella Atkins and Blair T. Mackiewich, "Fully Automatic Segmentation of Brain in MRI," IEEE Transactions on Medical Imaging, vol. 17, no. 1, pp. 98-107, February 1998.
- [3]. Atam P. Dhawan, Aleksandar Zavaljevski, Alok Sarwal, Walliam S. Ball, "A SYSTEM FOR MR BRAIN IMAGE SEGMENTATION," 18th Annual International Conference of the IEEE Engineering in Medicine and Biology Society, pp. 732-733 Amsterdam 1996.
- [4]. Laurent Verard, Jalal Fadili, Su Ruan, and Daniel Bloyet, "3D MRI SEGMENTATION OF BRAIN STRUCTURES," 18th Annual International Conference of the IEEE Engineering in Medicine and Biology Society, pp. 1081-1082 Amsterdam 1996.
- [5]. C. M. Wang, G. C. Lin, C. Y. Lin, and R. M. Chen, "An Unsupervised Kalman Filter-Based Linear Mixing Approach to MRI Classification," Proceedings of the 2004 IEEE Asia-Pacific Conference on Circuits and Systems, vol. 2, pp. 1105-1108, 6-9 Dec. 2004.
- [6]. C. M. Wang, C. C. C. Chen, S. C. Yang, P. C. Chung, Y. N. Chung, C. W. Yang, and C. I. Chang, "An Unsupervised Orthogonal Subspace Projection Approach to MR Image Classification," Optical Engineering, vol. 41, no. 7, pp. 1546-1557, Jul. 2002.

- [7]. C. M. Wang, S. C. Yang, P. C. Chung, C. I. Chang, C. S. Lo, C. C. Chen, C. W. Yang, and C. H. Wen, "Orthogonal Subspace Projection-Base Approaches to Classification of MR Images Sequences," *Computerized Medical Imaging and Graphics*, vol. 25, no. 6, pp. 465-476, Dec. 2001.
- [8]. M. C. Clark, L. O. Hall, D. B. Goldgof, L. P. Clarke, R. P. Velthuizen, and M. S. Silbiger, "MRI Segmentation using Fuzzy Clustering Techniques," *IEEE Engineering Med. Biol. Mag.*, pp. 730-742, Dec. 1994.
- [9]. M. N. Ahmed, S. M. Yamany, A. A. Farag, and T. Moriarty, "Bias Field Estimation and Adaptive Segmentation of MRI Data using a Modified Fuzzy C-means Algorithm," *IEEE Computer Society Conference on Computer Vision and Pattern Recognition*. vol. 1, pp. 250-255, Jun. 1999.
- [10]. M. N. Ahmed, S. M. Yamany, N. Mohamed, A. A. Farag, and T. Moriarty, "A Modified Fuzzy C-Means Algorithm for Bias Field Estimation and Segmentation of MRI Data," *IEEE Trans. on Medical Imaging*, vol. 21, no. 3, pp. 193-199, Mar. 2002.
- [11]. X. Du, Y. Li, and D. Yao, "A Support Vector Machine Based Algorithm for Magnetic Resonance Image Segmentation," *Fourth International Conference on Natural Computation*, 18-20 Oct. 2008.
- [12]. W. E. Reddick, J. O. Glass, E. N. Cook, T. D. Elkin, and R. J. Deaton, "Automated Segmentation and Classification of Multispectral Magnetic Resonance Images of Brain using Artificial Neural Networks," *IEEE Trans. on Medical Imaging*, vol. 16, no.6, pp. 911-918, Dec. 1997.
- [13]. J. S. Lin, R. M. Chen, and Y. M. Huang, "Medical Image Segmentation using Mean Field Annealing Network," *IEEE Conference on Image Processing*, vol. 2, pp. 855-858, Oct. 1997.
- [14]. J. Alirezaie, M. E. Jernigan, and C. Nahmias, "Automatic Segmentation of Cerebral MR Images using Artificial Neural Networks," *IEEE Trans. on Nuclear Science*, vol. 45, no. 4, pp. 2174-2182, Aug. 1998.
- [15]. J. S. Lin, K. S. Cheng, and C. W. Mao, "Multispectral Magnetic Resonance Images Segmentation using Fuzzy Hopfield Neural Network," *International Journal of Biomedical Computing*, pp. 205-214, Aug. 1996.
- [16]. A. Mayer, and H. Greenspan, "An Adaptive Mean-Shift Framework for MRI Brain Segmentation," *IEEE Trans. on Medical Imaging*, vol. 28, no. 8, pp. 1238-1250, Aug. 2009.
- [17]. A. Likas, N. Vlassis, and J. J. Verbeek, "The Global K-means Clustering Algorithm," *Pattern Recognition*, vol. 36, no. 2, pp. 451-461, Feb. 2003.
- [18]. C. M. Wang, C. Y. Lin, J. A. Lin, and Z. H. Zheng, "Application of Extenics Approach in MRI Classification," *18th IPPR Conference on Computer Vision, Graphics and Image Processing*, Taipei, Taiwan, pp. 15-20, Aug. 2005.
- [19]. J. C. Su, C. M. Wang, S. C. Yang, and G. H. Chang, "An Extenics Approach to MRI Classification," *2006 IEEE International Conference on Systems, Man, and Cybernetics*, Taipei, Taiwan, pp. 562-567, Oct. 2006.
- [20]. J. Kennedy, and R. Eberhart, "Particle swarm optimization," *IEEE Conf. on Neural Networks*, Perth, Australia, vol. 4, pp. 1942-1948, 1995.
- [21]. M. H. Wang, C. P. Hung, "Extension Neural Network and Its Applications," *Neural Networks*, vol. 16, no. 5-6, pp. 779-784, 2003.
- [22]. G. C. Lin, and W. J. Wang, "Multispectral MR images segmentation based on fuzzy knowledge and modified seeded region growing," *Magnetic Resonance Imaging*, vol. 30, no. 2, pp. 230-246, 2012.
- [23]. C. E. Metz, "ROC Methodology in Radiological Imaging," *Invest Radiol*, vol. 21, no. 9, pp. 720-723, Sep. 1986.



Chu-in-Mu Wang received his B.S. degree in Electronic Engineering from National Taipei Institute of Technology and his M.S. degree in Information Engineering from Tatung University of Taiwan in 1984 and 1990, respectively, and the Ph.D.

degree in Electrical Engineering from National Cheng-Kung University, Taiwan, ROC, in 2002. From 1984 to 1990, he was a system programmer on an IBM mainframe system and from 1990 to 1992 he was a marketing engineer on computer products at Tatung Company. Since 2002, he has been a professor at the National Chin-Yi University of Technology. His research interests include image processing, multispectral image processing, and medical imaging.



Shao-Wei Chu was born in Taichung, Taiwan, in 1985. He received the M.S. degree in Electronic Engineering from National Chin-Yi University of Technology in 2010. He is a Ph.D. student enrolled in Department of Computer Science and

Engineering in National Chung Hsing University. His research interests involve digital image processing, pattern recognition, and data mining.